# Direct determination by low-energy electron diffraction of the atomic structure of surface layers on a known substrate

A. Seubert and K. Heinz
*Lehrstuhl für Festkörperphysik, Universität Erlangen-Nürnberg, Staudtstraße 7, D-91058, Erlangen, Germany*

D. K. Saldin
*Department of Physics and Laboratory for Surface Studies, University of Wisconsin-Milwaukee, P.O. Box 413, Milwaukee, Wisconsin 53201*
(Received 30 October 2002; published 21 March 2003)

We develop a technique for the direct determination, by low-energy electron diffraction (LEED), of the atomic structure of surface layers on a known substrate. The key is the division of multiple-scattering paths into those that scatter solely from the known bulk of the sample and those that include scattering by a surface atom. In a holographic analogy, the sum of the contributions from the former may be identified with a (known) reference wave, and those from the surface with an (unknown) object wave. The latter may be written as a linear combination of elementary object waves, each of which may be regarded as a renormalized dynamical structure factor of a test two-dimensional (2D) superlattice of average atoms within a preselected 3D surface slab overlying the bulk crystal. The coefficients of this linear expansion, which may be determined by a maximum entropy algorithm, represent the 3D distribution of atoms within the surface slab. Examples are given of applications of the method for the determination of structures of adsorbates on known substrates from both simulated and experimental LEED data.

DOI: 10.1103/PhysRevB.67.125417 PACS number(s): 61.14.−x, 68.43.−h

## I. INTRODUCTION

One of the most successful tools for the determination of atomic arrangements at crystal surfaces is the technique of low energy electron diffraction (LEED).[1–3] In this technique, the angular and energy variations of backscattered low-energy electrons directed into a surface from the outside are monitored as a sensitive signature of the surface structure. The method relies on the short inelastic scattering length of electrons of such energy (usually in the range ~50–400 eV) for its surface sensitivity. However, similarly strong but elastic interactions of such electrons with materials are also responsible for a feature that adds considerably to the difficulty of relating the measured data to the surface structure, namely the fact that the electron scattering needs to be modelled by multiple-scattering theory.

Over the past several decades, such theories have been developed to the extent that *given a structure*, it is possible to accurately and quite swiftly calculate its complete LEED spectrum,[4] represented by intensity versus energy [or $I(E)$] variations of each of a number of measured Bragg spots. The current methodology for the determination of surface structures therefore is to calculate the expected LEED $I(E)$ spectra from a number of proposed model structures, and to search for the set that has the best fit to the corresponding experimental spectra as judged by a reliability factor ($R$ factor).[2]

As pointed out by Pendry, Heinz, and Oed,[5] this methodology runs into practically insuperable difficulties when an attempt is made to determine too many unknown structural parameters. The number of model structures, whose spectra would need to be calculated if $M$ different values of $N$ parameters are varied, is $M^N$, i.e., there is non-polynomial (NP) scaling.[5] If $c$ is the computer time needed for the calculation of a set of LEED spectra for a single model, then the time for the entire structure search would be $T=cM^N$. Substituting some typical numbers gives a concrete idea of the magnitude of the problem. Suppose one wished to determine the three Cartesian coordinates of $n$ surface atoms, then $N=3n$. Suppose also that each parameter was varied over $M=10$ discrete values. Then if $c=1$ second, and we required to determine the positions of just $n=3$ independent atoms, $T=10^9$ s≈30 years; for $n=6$, $T=10^{18}$ s≈$3\times10^{10}$ years, already about the age of the universe! An exhaustive search of models varying by a reasonable number of values of just a few parameters thus becomes practically impossible even with an orders of magnitude increases of computer speeds and/or the use of a reasonable number of parallel processors.

Guided search strategies to overcome this NP-complete problem in LEED have been developed including the use of gradient search methods,[6] simulated annealing,[7] frustrated simulated annealing,[8] and the genetic algorithm,[9] all of which improve on the disastrous exponential scaling with the number of parameters of the exhaustive search at the expense of some uncertainty regarding the attainment of the best global fit. Perturbation methods, like tensor LEED,[10] including automated versions,[11,12] require an initial guess of the structure fairly close to the true one.

An alternative approach that has been tried for rapid structure determination in LEED has exploited an analogy with *holography*.[13,14] In the technique of holographic LEED,[15,16] some of the diffracted amplitudes are considered to be a linear combination of a calculable *reference wave* arising from the scattering of an electron from an adatom on a crystal surface and an unknown *object wave* from the subsequent scattering of the same electron from a substrate of unknown structure. By interpreting a relevant subset of the LEED intensities as a *hologram*, a three-dimensional (3D) image of atoms near the adatom may be reconstructed from the data by a computer algorithm. This technique has been

 

applied successfully to experimental data,[17,18] and even to determine the local geometry around an adatom on the previously unknown SiC(111)$(3\times3)$ structure, which eventually enabled the full solution of that structure.[19] Nevertheless, a major limitation that holographic LEED shares with other forms of atomic-source electron holography[20] is that, due to the decay of the reference wave amplitude with the inverse of its distance from the source (augmented by a short inelastic mean free path), the recovered image is only of atoms within a rather local cluster around the adatom. This is usually not by itself sufficient to solve the structures of the larger surface unit cells.

The method we describe in this paper is also analogous to holography, but with the difference that the reference wave is regarded not as that scattering off a point adatom on a surface but from the entire known substrate that underlies the unknown surface to be determined. The object wave arises not from the subsequent scattering of a point scattering source, but from the direct scattering of the incident electrons from the unknown surface region (and other contributions from paths including, in addition, scattering from atoms in the substrate). All surface atoms contribute to the object wave with a strength more or less independent of their position in their unit cell, and their positions might thus all be equally expected to be determined. The method is closely analogous to one already developed for the structure completion problem of protein crystallography,[21] and for a similar problem in surface x-ray diffraction,[22] both of which may be adequately treated by a single-scattering (or kinematic) theory. We show in the present paper how the method may be adapted even for the strong multiple-scattering problem of LEED, and point out its near-ideal scaling properties with the complexity of the surface structure. A preliminary account of this work has already been published.[23]

## II. OUTLINE OF THE THEORY

We begin with an outline of the theory, whose details will be given in the following sections. LEED is an experiment in which electrons are directed into a sample from a distant source and the intensities of elastically backscattered electrons suffering different momentum transfers **g** parallel to the surface are monitored. In the case of a crystal surface, nonzero diffracted intensities will be found only when **g** is a 2D reciprocal-lattice vector of the surface, i.e., when

$$\mathbf{g}=H\mathbf{a}^*+K\mathbf{b}^*. \tag{1}$$

If $\mathbf{a}^*$ and $\mathbf{b}^*$ are surface parallel reciprocal-lattice unit-cell vectors defined by the substrate, and when there is no surface reconstruction, allowable values of **g** correspond to only integer values of the Miller indices $H$ and $K$. The Bragg spots on a detector corresponding to such values of $H$ and $K$ are known as *integer-order* spots. If the surface structure is reconstructed, atoms in the outermost surface layers may rearrange themselves to form a 2D lattice of larger linear dimensions than the deeper layers parallel to the surface. In such a case, or if foreign atoms or molecules from a periodic overlayer of such a larger lattice parameter on the surface, LEED electrons may be backscattered also into so-called *fractional-order* Bragg spots with surface-parallel momentum transfers **g** given by fractional values of the Miller indices $H$ or $K$ in Eq. (1).

A LEED experiment measures the backscattered intensities of a set of Bragg reflections **g** as a function of the energy $E$ of the incident electrons. Each intensity measurement $I_\epsilon$ may thus be specified by an index $\epsilon$ representing a combination of diffracted beam **g** and electron energy $E$. These intensities are proportional to the squares of the moduli of the corresponding structure factors $F_\epsilon$ of a 2D repeating unit of the structure (or unit cell).

The approach we will follow has the following three key ingredients. First, the above structure factor is regarded as the sum of two components

$$F_\epsilon=R_\epsilon+S_\epsilon, \tag{2}$$

where $R_\epsilon$ incorporates all possible multiple scattering paths of the incident electron with the known part of the surface, namely the deeper layers, whose structure is essentially that of the bulk crystal. $S_\epsilon$ represents the effect of all multiple-scattering paths that include (but are not restricted to) scattering from the unknown part, namely, the outermost atomic layers, whose structure is to be determined. It should be noted that although, in general, the integer-order Bragg spots have nonzero contributions from both $R_\epsilon$ and $S_\epsilon$, the fractional-order spots are comprised entirely of $S_\epsilon$. The decomposition [Eq. (2)] of $F_\epsilon$ is very analogous to *holography*,[13] where $R_\epsilon$ and $S_\epsilon$ may be regarded as complex reference and object waves, respectively, interfering to form a hologram, represented by the set of real intensities $\{I_\epsilon\}$.

The second ingredient is the fact that in LEED, to a very good approximation, it is possible to express $S_\epsilon$ in the form

$$S_\epsilon=\sum_l p_l O_{\epsilon l}, \tag{3}$$

where $O_{\epsilon l}$ represents a *renormalized scattering matrix* (in a plane-wave representation) of a primitive 2D test superlattice, which includes an *average atom* at a position $l$. Here we use the term average atom in the same sense that it is used in the *direct methods*[24] of x-ray crystallography: namely, it is an atom whose scattering properties are an average of those of the atoms expected in a surface slab of area equal to that of the superlattice, and a depth estimated to contain all the atoms of the surface region, whose positions are unknown at the outset. The term renormalized above implies that included in the calculation of this matrix is the dominant multiple-scattering between the substrate and the unit cell of the resulting *test layer* of average atoms. It may be regarded as a form of an *elementary object wave*,[25] which may be calculated without a knowledge of the surface structure. Thus the total object wave $S_\epsilon$ may be regarded as a linear combination of calculable elementary object waves, with a set of real and non-negative expansion coefficients $p_l$. This representation of $S_\epsilon$ is an approximation that neglects multiple scattering between the sublattices represented by the quantities $O_{\epsilon l}$. As we will see in the following, even in the rather severe test of LEED electrons normally incident on a

surface containing normally-oriented CO molecules this appears to be a good enough approximation.

Our idea is to define the real-space distribution $\{p_l\}$ on a uniform 3D Cartesian grid covering a lateral extent equal to that of the surface unit cell and of a height sufficient to include all the expected surface atoms. The third ingredient of our theory is the use of a maximum entropy algorithm to determine the distribution $\{p_l\}$ from the experimental data. Peaks in this distribution would indicate the likely positions of atoms in the surface slab. The basic idea of the maximum entropy method is described next.

### III. MAXIMUM ENTROPY METHOD

The problem of obtaining stable and meaningful solutions from incomplete and noisy data has been addressed in a variety of fields by means of the principles of Bayesian statistics,[26] and the maximum entropy method in particular.[27,28] In x-ray crystallography, this idea has been used to develop an *exponential modeling* algorithm[29,30] for improving the resolution of a pre-existing electron density map of a protein. A similar exponential modelling scheme has been used[31–34] as part of an iterative process of *phase extension*, in which a knowledge of the phases of some low-resolution structure factors is extended to those of higher resolution shells.[35]

A maximum entropy algorithm, developed originally to improve the resolution of protein electron density maps,[29] has been adapted to solve the problem of structure completion in protein crystallography[21] and surface x-ray diffraction.[22] We now develop an adaptation of this theory to determine the sought atom distribution $\{p_l\}$. We begin by defining the entropy of this distribution using Boltzmann's expression

$$\mathcal{S}[\{p_l\}] = k \ln[\Omega\{p_l\}], \tag{4}$$

where $k$ is Boltzmann's constant, and the number of microstates per macrostate, $\Omega$, is proportional to the probability ($P$) of the distribution. Consequently,

$$P[\{p_l\}] \propto \exp \mathcal{S}[\{p_l\}]. \tag{5}$$

Thus the most probable distribution $\{p_l\}$ corresponds to that which maximizes $S$. A convenient form for the entropy, which is equivalent to Boltzmann's expression above, is the Gibbs' form[36]

$$\mathcal{S}[\{p_l\}] = -\sum_l p_l \ln \frac{p_l}{e m_l}, \tag{6}$$

where $e$ the base of the natural logarithms, and $\{m_l\}$ the best prior guess of the optimum distribution $\{p_l\}$ (which we could term the measure of the distribution). By differentiating $\mathcal{S}$ with respect to $p_j$ (where $j$ is a particular one of the set of indices $\{l\}$) it is easy to show that the distribution $\{p_l\}$ that maximizes $\mathcal{S}$ is the trivial one that is identical to $\{m_l\}$.

For our problem of finding the most probable electron distribution $\{p_l\}$ consistent with the experimental data, we need to constrain the distribution by the method of Lagrange multipliers. In our present application, we identify $\{p_l\}$ with our best guess of the distribution $\{p_l^{(n)}\}$ of the unknown part of a unit cell at step $n$ of an iterative algorithm. We identify the measure $\{m_l\}$ with our estimate $\{p_l^{(n-1)}\}$ of the electron distribution at the previous iteration. We seek to maximize the functional,

$$Q[\{p_l^{(n)}\}] = -\sum_l p_l^{(n)} \ln\left[\frac{p_l^{(n)}}{e p_l^{(n-1)}}\right] - \frac{\lambda'}{2}\chi^2, \tag{7}$$

where the first term represents the entropy of the distribution $\{p_l^{(n)}\}$ at an iteration $n$, relative to one $\{p_l^{(n-1)}\}$ at the previous iteration, and the second term is proportional to the $\chi^2$ statistic,

$$\chi^2 = \frac{1}{N}\sum_\epsilon \frac{|F_\epsilon^{(c)(n)} - c^{(n-1)} F_\epsilon^{(o)(n-1)}|^2}{\sigma_\epsilon^2}, \tag{8}$$

with $\sigma_\epsilon$ the estimated uncertainty in the measured structure factor amplitude $|F_\epsilon|$, $N$ the number of data points $\epsilon$, and $\lambda'$ a Lagrange multiplier. This quantifies the agreement, at the $n^{\text{th}}$ iteration of the algorithm, between the set of calculated structure factors,

$$F_\epsilon^{(c)(n)} = R_\epsilon + S_\epsilon^{(n)}, \tag{9}$$

where

$$S_\epsilon^{(n)} = \sum_l p_l^{(n)} O_{\epsilon l}, \tag{10}$$

with the corresponding observed structure factors,

$$F_\epsilon^{(o)(n-1)} = |F_\epsilon| \exp[i\phi_\epsilon^{(n-1)}], \tag{11}$$

where the phase of this structure factor is equated to that of the calculated one at the previous iteration, i.e., with

$$\phi_\epsilon^{(n-1)} = \arg[F_\epsilon^{(c)(n-1)}]. \tag{12}$$

The purpose of the real constant $c^{(n-1)}$ in Eq. (8) is to scale the observed structure factor $|F_\epsilon^{(o)}|$ to match that of its calculated counterpart at each iteration via the equation:

$$c^{(n-1)} = \frac{\Sigma_\epsilon |F_\epsilon^{(c)(n-1)}|}{\Sigma_\epsilon |F_\epsilon^{(o)(n-1)}|}. \tag{13}$$

The quantity $Q$ in Eq. (8) may be maximized by requiring that

$$\frac{\partial Q}{\partial p_j^{(n)}} = 0, \quad \forall j. \tag{14}$$

The differentiation of the entropy term in Eq. (7) is straightforward enough; that of the constraint term may be performed by writing $|F_\epsilon^{(c)(n)} - c^{(n-1)} F_\epsilon^{(o)(n-1)}|^2$ as $\{F_\epsilon^{(c)(n)} - c^{(n-1)} F_\epsilon^{(o)(n-1)}\}$ times its complex conjugate and noting that $F_\epsilon^{(c)(n)}$ depends on $p_l^{(n)}$, but not $F_\epsilon^{(o)(n-1)}$. After some algebra we obtain

$$\ln\left[\frac{p_j^{(n)}}{p_j^{(n-1)}}\right] = -\lambda' \frac{1}{N} \mathrm{Re} \sum_\epsilon \frac{1}{\sigma_\epsilon^2} \{F_\epsilon^{(c)(n)} - c^{(n-1)} F_\epsilon^{(o)(n-1)}\} O_{\epsilon j}^* . \quad (15)$$

If the individual variances $\sigma_\epsilon^2$ may be replaced by their mean value $\langle \sigma_\epsilon^2 \rangle$, we may define $\lambda = \lambda'/N \langle \sigma_\epsilon^2 \rangle$ and re-express Eq. (15) as

$$p_j^{(n)} = p_j^{(n-1)} \exp\left[ -\lambda \, \mathrm{Re} \sum_\epsilon \{F_\epsilon^{(c)(n)} - c^{(n-1)} F_\epsilon^{(o)(n-1)}\} O_{\epsilon j}^* \right], \quad \forall j. \quad (16)$$

Substituting for $F_\epsilon^{(c)(n)}$ from Eq. (9), we see that Eqs. (16) represent a set of *implicit* equations for the sought distribution $\{p_j^{(n)}\}$ at the $n$th iteration in terms of that $\{p_j^{(n-1)}\}$ at the previous iteration.

If $\lambda$ were chosen to be sufficiently small, the change of $\{p_j^{(n)}\}$ per iteration will be small enough to justify the replacement of $F_\epsilon^{(c)(n)}$ by its value $F_\epsilon^{(c)(n-1)}$ at the previous step. By analogy with the corresponding algorithm for x-ray diffraction,[21,22] one may argue that $\lambda$ needs to satisfy a condition of the form

$$\lambda^{(n-1)} \ll \frac{b}{\max(\{p_l^{(n-1)}\})}, \quad (17)$$

where $\max\{p_l^{(n-1)}\}$ is the maximum value of the distribution $\{p_l^{(n-1)}\}$ at iteration $(n-1)$, and $b$ is a constant. Equations (16) may then be replaced by the set of *explicit* equations

$$p_j^{(n)} = p_j^{(n-1)} \exp\left[ -\lambda^{(n-1)} \mathrm{Re} \sum_\epsilon \{F_\epsilon^{(c)(n-1)} - c^{(n-1)} F_\epsilon^{(o)(n-1)}\} O_{\epsilon j}^* \right], \quad \forall j, \quad (18)$$

which, together with Eqs. (9)–(12), constitute a well-defined set of recursion relations which transform an arbitrarily chosen initial distribution $\{p_j^{(0)}\}$ at iteration $n=1$ to a final converged distribution $\{p_j^{(m)}\}$ at iteration $m$ that constitutes the best estimate of the distribution of average atoms in the surface slab.

In the absence of any knowledge of this distribution at the outset, a reasonable starting distribution is a uniform one normalized to the expected number $N_{\mathrm{atom}}$ of atoms in the surface unit cell. That is, one may take

$$p_j^{(0)} = \frac{N_{\mathrm{atom}}}{N_{\mathrm{vox}}}, \quad \forall j \quad (19)$$

where $N_{\mathrm{vox}}$ is the number of voxels at which the distributions $\{p_j^{(n)}\}$ are evaluated. After completion of each iteration, the new distribution is renormalized by the condition

$$\sum_j p_j^{(n)} = N_{\mathrm{atom}} . \quad (20)$$

An initial estimate of the calculated structure factor $F_\epsilon^{(o)(0)}$ requires initial estimates of the phases $\phi_\epsilon^{(0)}$ which may be calculated by Eq. (12) at least for the integer-order beams. However, as already outlined in Secs. II, although integer-order Bragg spots always have a contribution not only from the surface $S_\epsilon$ but also from the known bulk structure (through $R_\epsilon$), superstructure Bragg spots do not. Therefore, a special treatment of the initial corresponding phases is necessary. To this aim the algorithm first operates on the structure factor amplitudes of the integer-order spots only, until an intermediate convergence after $n_1$ iterations is reached. The distribution $\{p_l^{(n_1)}\}$ obtained at this stage gives rise to the so-called *average* or *folded* structure (cf. Secs. II and V). The recovery of the true superstructure periodicity then comes by the inclusion of the amplitudes of the fractional-order spots. As a starting point, their phases are approximated by a linear interpolation between the estimates of the phases of their neighboring integer-order spots of the same electron energy at iteration step $n_1$. With the inclusion of the data of the superstructure spots, the algorithm is then resumed until its final convergence, where from iteration $(n_1+1)$ on both the integer-order and fractional-order phases are determined iteratively by Eq. (12).

## IV. FORM OF HOLOGRAPHIC REFERENCE AND OBJECT WAVES

We now turn to the question of the form of $R_\epsilon$ and $O_{\epsilon j}$ for a workable algorithm for LEED. For a key to an understanding of this, first consider the evaluation of the scattering of a LEED electron from a surface consisting of an ordered 2D test layer of the periodicity of the superlattice above a crystal substrate. We assume that the structure of the substrate is known, and that thus it is possible to calculate exactly its reflection matrix $\mathbf{B}^{-+}$ in a plane-wave basis. If the ''in-out'' scattering matrix of the test layer (in the same basis) is defined as $\mathbf{M}^{-+}$, the ''in-in'' matrix as $\mathbf{M}^{++}$, and the ''out-out'' matrix as $\mathbf{M}^{--}$ in the usual LEED notation, where the second superscript denotes the direction from which a wave is incident on the layer or substrate, and the first one that of the scattered (or transmitted) wave. The superscript $+$ indicates a direction of flux from vacuum into the surface, and—the reverse flux. Exploiting the weakness of backscattering processes compared to forward-scattering ones, the scattering paths involving the adsorbate layer and substrate may be ordered by the number of backscattering processes involved. Obviously, the minimum number of backscattering processes for the detection of a flux of backscattered LEED electrons above the surface is one. Also, exploiting the weakness of $\sim 90°$ scattering of LEED electrons of normal incidence compared with either forward scattering or backscattering, we approximate the scattering matrices $\mathbf{M}^{\pm\pm}$ by ''kinematic'' expressions,[1] that neglect multiple scattering within the adlayer.[37]

Suppose that the outer edges of the surface atoms extend to a height $h$ above the uppermost atomic layer of the substrate (see Fig. 1). The plane parallel to the surface at this height may then be regarded as the interface between the

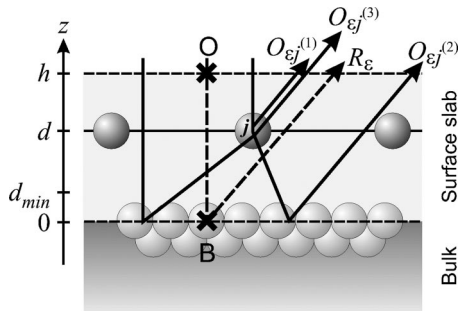


FIG. 1. Propagation and scattering paths giving rise to the reference wave $R_\epsilon$ and the three dominant contributions $O_{\epsilon j}^{(1)}$, $O_{\epsilon j}^{(2)}$, and $O_{\epsilon j}^{(3)}$ to the object wave $O_{\epsilon j}$. The surface atomic layer is assumed to extend to a height $h$ above the bulk with its origin at point $j$ at height $d$ above the bulk. $O$ is the real-space origin with respect to which all mutually coherent paths are referenced, $B$ denotes the conventional origin for the calculation of the bulk reflection matrix $\mathbf{B}^{-+}$.

sample and the vacuum. The propagation of electrons below this layer must take account of both refraction and absorption. Thus, it is convenient to define an origin $O$ at some reference point in this interface plane, with respect to which is measured the phase of a plane wave of unit amplitude representing the incident LEED electron. We also define an origin $j$ of the adsorbate layer, taken at the position of an atom in the test layer, and in a plane of height $d_{\min} \leqslant d \leqslant h$ above the outermost substrate layer. (The definition of a lower boundary $d_{\min} \approx 1$ Å of the surface slab is necessary to ensure the validity of the renormalized scattering matrix approximation.) Also, we define $B$ to be the conventional origin assumed for the definition of the bulk reflection matrix $\mathbf{B}^{-+}$. Let the propagation matrix (also in the plane wave representation) of an electron from $O$ to $j$ be defined as $\mathbf{P}_{jO}$, that from $j$ to $B$ be $\mathbf{P}_{Bj}$, and the corresponding propagation matrices in the reverse directions be $\mathbf{P}_{Oj}$ and $\mathbf{P}_{jB}$, respectively. Then the total reflection matrix of the entire surface to first-order in backscattering may be written

$$\mathbf{T} = \mathbf{P}_{Oj}\mathbf{M}^{-+}\mathbf{P}_{jO} + \mathbf{P}_{Oj}(\mathbf{1}+\mathbf{M}^{--})\mathbf{P}_{jB}\mathbf{B}^{-+}\mathbf{P}_{Bj}(\mathbf{1}+\mathbf{M}^{++})\mathbf{P}_{jO} \tag{21}$$

$$\begin{aligned} &= \mathbf{P}_{Oj}\mathbf{P}_{jB}\mathbf{B}^{-+}\mathbf{P}_{Bj}\mathbf{P}_{jO} + \mathbf{P}_{Oj}\mathbf{M}^{-+}\mathbf{P}_{jO} \\ &\quad + \mathbf{P}_{OB}\mathbf{B}^{-+}\mathbf{P}_{Bj}\mathbf{M}^{++}\mathbf{P}_{jO} + \mathbf{P}_{Oj}\mathbf{M}^{--}\mathbf{P}_{jB}\mathbf{B}^{-+}\mathbf{P}_{BO} \\ &\quad + \mathbf{P}_{Oj}\mathbf{M}^{--}\mathbf{P}_{jB}\mathbf{B}^{-+}\mathbf{P}_{Bj}\mathbf{M}^{++}\mathbf{P}_{jO}, \end{aligned} \tag{22}$$

where unit matrices **1** are added to the ''in-in'' and ''out-out'' matrices to take account of unscattered transmission. Since the product of two free-space propagator matrices involving an intermediate point is independent of that intermediate point,

$$\mathbf{P}_{BO} = \mathbf{P}_{Bj}\mathbf{P}_{jO} \tag{23}$$

and

$$\mathbf{P}_{OB} = \mathbf{P}_{Oj}\mathbf{P}_{jB}. \tag{24}$$

From these relations, we see that the first term on the right-hand side of Eq. (22) above is independent of the surface layer. One of its elements forms a suitable reference wave for our purposes, namely,

$$R_\epsilon = (\mathbf{P}_{OB}\mathbf{B}^{-+}\mathbf{P}_{BO})_{\mathbf{g0}}, \tag{25}$$

where the indices **g0** specify the matrix elements for scattering from an incident wave to the backscattered Bragg reflection labeled by the reciprocal-lattice vector **g**. The remaining terms on the right-hand side of (22) enable the calculation of the corresponding object wave via

$$\begin{aligned} O_{\epsilon j} &= (\mathbf{P}_{Oj}\mathbf{M}^{-+}\mathbf{P}_{jO} + \mathbf{P}_{OB}\mathbf{B}^{-+}\mathbf{P}_{Bj}\mathbf{M}^{++}\mathbf{P}_{jO} \\ &\quad + \mathbf{P}_{Oj}\mathbf{M}^{--}\mathbf{P}_{jB}\mathbf{B}^{-+}\mathbf{P}_{BO} \\ &\quad + \mathbf{P}_{Oj}\mathbf{M}^{--}\mathbf{P}_{jB}\mathbf{B}^{-+}\mathbf{P}_{Bj}\mathbf{M}^{++}\mathbf{P}_{jO})_{\mathbf{g0}} \\ &\simeq O_{\epsilon j}^{(1)} + O_{\epsilon j}^{(2)} + O_{\epsilon j}^{(3)}, \end{aligned} \tag{26}$$

where

$$O_{\epsilon j}^{(1)} = (\mathbf{P}_{Oj}\mathbf{M}^{-+}\mathbf{P}_{jO})_{\mathbf{g0}}, \tag{27}$$

$$O_{\epsilon j}^{(2)} = (\mathbf{P}_{OB}\mathbf{B}^{-+}\mathbf{P}_{Bj}\mathbf{M}^{++}\mathbf{P}_{jO})_{\mathbf{g0}}, \tag{28}$$

and

$$O_{\epsilon j}^{(3)} = (\mathbf{P}_{Oj}\mathbf{M}^{--}\mathbf{P}_{jB}\mathbf{B}^{-+}\mathbf{P}_{BO})_{\mathbf{g0}}, \tag{29}$$

with the fourth term involving the product of the scattering matrices $\mathbf{M}^{--}$ and $\mathbf{M}^{++}$ neglected.

The use of the reference and elementary object waves in the form of Eqs. (25) and (26), respectively, certainly is an approximation, It is justified if substitution of these expressions into Eqs. (3) and (2) would give a reasonable approximation to the dynamical LEED structure factor $F_\epsilon$ for a distribution $\{p_j\}$ of atom positions within a surface unit cell, to be determined by the iterative algorithm of the last section. An assumption of this approximation is that multiple scattering between different surface atoms may be neglected. Due to the predominantly forward-scattering nature of atomic scattering factors for LEED electrons, this is usually a good approximation for normally-incident electrons and adsorbates confined to a single layer parallel to the surface.[37]

The following test computations illustrate the reasonableness of these approximations: the results of a full dynamical intensity calculation for the artificial structure of a primitive oxygen layer with $c(2\times2)$ periodicity 2 Å above a Ni(001) surface with the oxygen atoms on on-top sites of the Ni substrate were compared with the $I(E)$ curves computed on the bases of these approximations. The results are shown in Fig. 2 for a selected integer- and fractional-order beam. Representative scattering paths followed by electrons contributing to $R_\epsilon$, $O_{\epsilon j}^{(1)}$, $O_{\epsilon j}^{(2)}$, and $O_{\epsilon j}^{(3)}$ are illustrated in Fig. 1.

## V. RESULTS FROM SIMULATED LEED DATA

Our initial test of the method was on data simulated by a standard LEED program.[4] An attempt was made to recover from this data the surface structure model assumed in the simulation of the LEED $I/E$ curves.

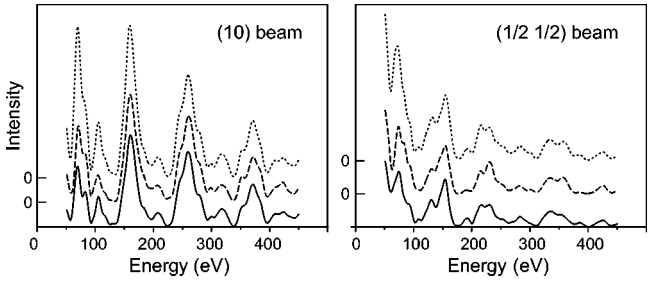


FIG. 2. Full dynamic intensities (solid lines) calculated for $c(2\times2)$-O/Ni(001) and compared with calculations based on the neglect of intralayer multiple scattering within the test layer (dashed line), and this approximation plus the representation of **T** by just the first four terms on the right-hand side of Eq. (22) (dotted lines).

### $c(2\times2)$-CO/Ni(001)

The model chosen is that accepted for $c(2\times2)$CO/Ni(001) with the CO molecules adsorbed perpendicular to the surface and the C atom residing in on-top sites of the Ni substrate as shown in Fig. 3. The simulated data input to the algorithm were $I(E)$ spectra calculated for normal electron incidence and an energy range of 30 eV up to 450 eV for the five inequivalent integer-order Bragg reflections (10), (11), (20), (21), and (22) and the five inequivalent half-order reflections (1/2 1/2), (3/2 1/2), (3/2 3/2), (5/2 1/2), and (5/2 3/2), which should all be easily accessible from experiment. Also given as input to the algorithm were the complex amplitudes $R_\epsilon$ from bulk Ni(001), calculated from the dynamical structure factors, $\mathbf{B}^{-+}$, of the substrate by the same program. The computations of the propagation matrices, e.g., $\mathbf{P}_{jO}$, for the evaluation of $R_\epsilon$ and $O_{\epsilon j}$ from Eqs. (25) and (26), respectively, require only the evaluation of complex exponentials with arguments containing the (complex) wave vectors of the plane-wave expansions between the atomic layers and the vectors relating the fixed reference positions *O* and *B*, and the test positions *j* of atoms within a surface unit cell.

Figure 4 shows the calculated $I(E)$ spectrum of the (10) beam (solid line) for $c(2\times2)$-CO/Ni(001) in an energy range from about 100 to 400 eV, assuming atop adsorption of CO directly above each of the Ni atoms in the outermost substrate layer. The Ni-C distance was taken to be 1.8 Å, the

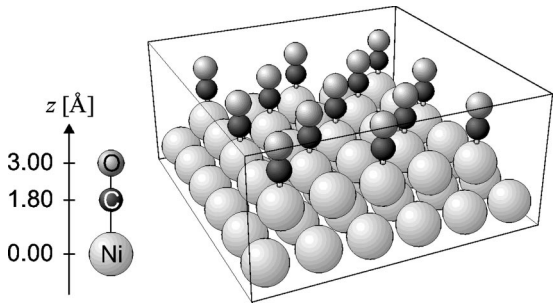


FIG. 3. Model of the $c(2\times2)$-CO/Ni(001) surface. The CO molecules are adsorbed on-top of Ni atoms. Their orientation is perpendicular to the surface with the *C* atoms coordinated to the outermost Ni atoms of the substrate.

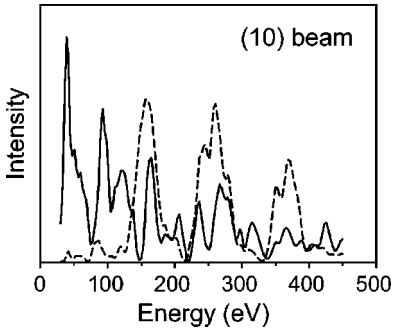


FIG. 4. $I(E)$ spectra of the (10) beam calculated for $c(2\times2)$-CO/Ni(001) (solid line) and for the clean Ni(001) surface (broken line). In both cases the same origin is chosen (3.2 Å above the outermost Ni layer).

C-O distance 1.2 Å, and the height *h* of the origin *O* above the outermost Ni layer taken to be 3.20 Å. The square roots of the intensities of this structure are the structure factor amplitudes $|F_\epsilon|$ used as input to the algorithm of Sec. III. Also shown as a dashed line in Fig. 4 is the intensity from a clean Ni(001) surface for the same position of the origin *O* relative to the Ni atoms.[38] These intensities are equal to $|R_\epsilon|^2$, where the quantities $R_\epsilon$ are the calculated complex amplitudes representing the reference waves, also used as input to the algorithm.

With the above definition of the reference waves $R_\epsilon$, the algorithm is applied to recover the positions of the CO overlayer relative to the Ni substrate. As stated earlier, in general, the method would deal with the circumstance of the adsorbates containing atoms of two different chemical species by computing the scattering matrices $\mathbf{M}^{++}$ of the test layer from average *t* matrices of atoms of these two species. In the present case, however, the atomic numbers, and hence *t*-matrices of the C and O species are so close that we took as our test layer one consisting of just a 2D oxygen superlattice of $c(2\times2)$ periodicity relative to the substrate.

We assumed an initial distribution $\{p_j^{(0)}\}$ to be the least-biased uniform one [Eq. (19)], normalized to the expected number $N_{\text{atom}}=2$ of atoms in a unit cell of the surface slab with height $h=3.20$ Å ($d_{\min}=1.0$ Å) on a 0.20-Å grid and a lateral extension of $-2.85$ to $+2.85$ Å with a resolution of 0.15 Å in both *x* and *y* directions. The algorithm (with λ set to 0.5) was run initially with the summation over $\epsilon$ in Eq. (18) only over data of the integer-order Bragg spots. The distribution $\{p_j^{(60)}\}$ resulting after 60 iterations is shown in the left panel of Fig. 5. This has the same periodicity parallel to the surface as the substrate, and reveals two high-intensity features on all on-top sites corresponding to the expected heights above the surface of the constituent atoms of upright CO molecules. This corresponds to what has been termed the *average*[22] or *folded*[39] structure in surface x-ray diffraction. It represents the *average* of the surface structures above all bulk unit cells *folded* into a surface unit cell of lateral dimensions equal to that of a bulk unit cell.

At this point, data from the fractional-order Bragg spots were also included in the summation over $\epsilon$ in Eq. (18). Initial phases $\phi_\epsilon^{(60)}$ of the fractional-order structure factors were taken to be values interpolated from the current results

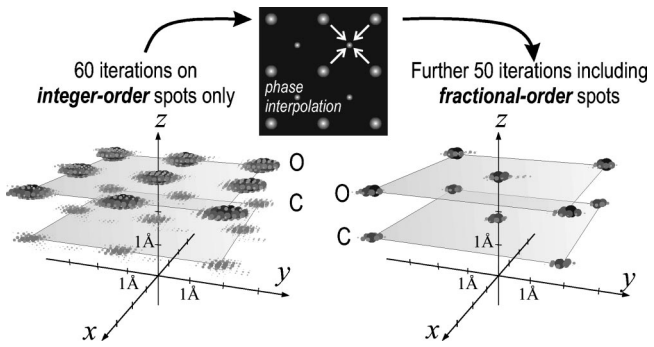


FIG. 5. Perspective atomic images reconstructed for $c(2\times2)$-CO/Ni(100). Transparent surface-parallel planes through the atoms imaged at $z\approx1.8$ Å (C) and 3.0 Å (O) are introduced to guide the eye. The bulk starts at $z=0$. Left: Image recovered after 60 iteration steps using substrate spot data only and producing a $1\times1$ overlayer of CO molecules. Middle: Procedure to obtain a first estimate for the superstructure phases by linear interpolation between phases of neighboring substrate spots. Right: $c(2\times2)$ arrangement of CO recovered after further 50 iterations, also including fractional order spots.

for the phases of the surface components, $S_\epsilon^{(60)}$, of the structure factors of the nearest-neighbor integer-order Bragg spots in the diffraction pattern at the same energy, as indicated in the middle panel of Fig. 5.

The distribution $\{p_j^{(110)}\}$ after a further 50 iterations is shown in perspective in the right panel of Fig. 5. Views of this distribution from directions parallel and normal to the surface (side elevation and plan views, respectively) are shown in Fig. 6, in which the atoms of the two topmost Ni(001) layers (the reference structure) are added artificially as hard spheres. The most obvious difference with the distribution of Fig. 5 (left) is that the CO molecules now appear adsorbed only on on-top sites of a $c(2\times2)$ lattice. The intensities associated with the two atoms in each adsorbed molecule are now approximately equal. The short horizontal lines on the left of the side elevation in Fig. 6 mark the heights of the C and O atoms above the surface assumed in the surface structure model. The computed distribution is thus seen to represent the correct recovery from the data of the complete structure of the CO molecules on the Ni(001) surface assumed in the model from which the LEED data were calculated.

This test of our algorithm with simulated LEED data enables us to test the effectiveness of the algorithm in recovering the correct phases of the dynamical structure factors. Monitoring the average phase difference between the estimated and correct phases,

$$\Delta\phi^{(n)}=\frac{1}{N}\sum_{\epsilon}|\phi_\epsilon^{(\mathrm{corr})}-\phi_\epsilon^{(n)}|, \tag{30}$$

provides useful information on the progress of the iterative procedure. For the $c(2\times2)$-CO/Ni(001) structure under consideration, the variation of this quantity is displayed in the left hand panel of Fig. 7. Starting with an initial value of about 66°, the average phase difference decreases until the intermediate convergence at iteration $n_1=60$ is reached. At

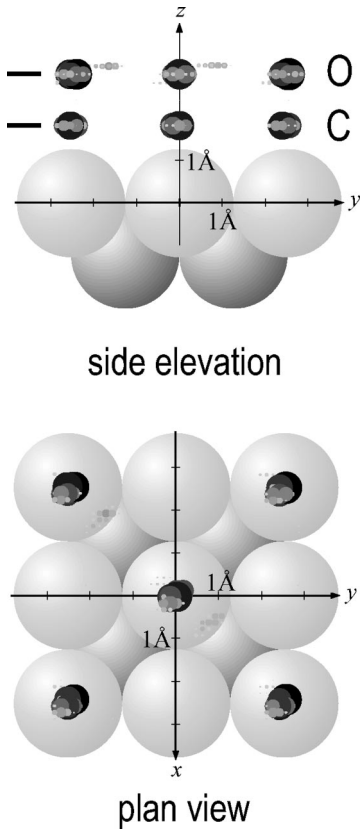


FIG. 6. Plan view and side elevation of the final result for $c(2\times2)$-CO/Ni(100) according to the right panel in Fig. 5.

this stage the fractional-order spots are included for the first time; the summation in Eq. (30) therefore comprises both groups of reflections. Of course, the simple linear interpolation procedure between neighboring integer-order spots may not be expected to provide accurate first estimates of the superstructure phases. This gives rise to the spike at iteration $n=n_1+1$. However, only a few further iterations make $\Delta\phi^{(n)}$ decrease again to about the same level that has been reached when the algorithm operated on the integer-order spots only.

In view of the very clearly and accurately recovered atomic distribution within the surface slab (cf. Figs. 5 and 6), the overall level of the average phase difference is rather high. The reason of this unsettling detail may be found in the approximations made for the calculation of the object wave

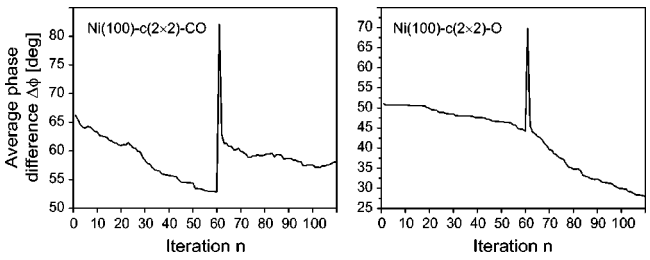


FIG. 7. Dependency of the average phase difference $\Delta\phi^{(n)}$ on the iteration step $n$ for $c(2\times2)$-CO/Ni(001) (left panel) and $c(2\times2)$-O/Ni(001) (right panel). See the text for details.

$S_\epsilon$. First, the total reflection matrix of the entire surface slab is correct only to first order in backscattering [cf. Eqs. (21) and (22)]. Second, multiple scattering *within* the surface slab, i.e., between different surface atoms, is neglected at all. Of course, the latter is a rather severe approximation, in particular for the worst-case scenario of the primary beam normally incident on the $c(2\times2)$-CO/Ni(001) structure with their CO molecules aligned perpendicularly to the surface. This effect is lifted when only a single adsorbed layer is used instead of the CO double layer. To this end, we performed another full dynamic calculation for the same structure but with the carbon layer removed, corresponding to $c(2\times2)$-O/Ni(100) with oxygen atoms 2.0 Å above the topmost Ni atoms. As can be seen in the right hand panel of Fig. 7, the overall level of the average phase difference now is much lower than for the case of the CO structure with a final value of less the 30°.

Due to the approximations made for the calculation of the object wave, it would not be surprising if $\Delta\phi^{(n)}$ never decreased significantly below this level. The successful recovery of the $c(2\times2)$-CO/Ni(001) structure in this section shows that even for the case of rather strong multiple scattering and a relatively high level of phase difference the algorithm still works reliably.

## VI. RESULTS FROM EXPERIMENTAL LEED DATA

For tests of the algorithm on experimental LEED data, we chose three systems whose structures have recently been determined by conventional LEED with high accuracy. These are two different phases of Br adsorbed on Pt(110), and a H adsorbate-induced reconstruction of Ir(001).

### A. $c(2\times2)$-Br/Pt(110)

The $c(2\times2)$ phase of Br/Pt(110) has been the subject of intense studies by scanning tunneling microscopy, (STM) total energy calculations using density functional theory (DFT), and quantitative conventional LEED.[40] Both DFT and LEED found Br atoms adsorbed in short-bridge sites with some slight adsorbed induced substrate reconstruction involved. However, an exhaustive structural search had to be applied as also other sites and, in particular, also substitutional sites had to be tested according to earlier suggestions.[41]

In contrast, as first described in our recent paper,[23] our method allows a *model-independent* determination of the adsorption geometry from the same data. Neglecting the small reconstruction of the substrate, the reference wave $R_\epsilon$ was computed from Eq. (25) with $\mathbf{B}^{-+}$ from a LEED calculation from an ideal bulk-terminated model of the Pt(110) substrate, and a surface slab height of 2.40 Å (again, $d_{\min}=1.0$ Å). The lateral extension of the surface slab ranges from $-4.40$ to $+4.40$ Å, with a resolution of 0.20 Å, and so covers a little more than a $c(2\times2)$ surface unit cell. The algorithm (with λ set to 0.5) was run to convergence after 350 iterations with just the data of the eight lowest-indexed integer-order Bragg spots included in the summation over $\epsilon$ in Eq. (18). Initial phases were then assigned to the four lowest-indexed fractional-order structure factors by the same reciprocal-space interpolation from the surface components of the structure factors of the integer-order spots, as described in the last subsection. The algorithm was resumed with data from both integer-order and fractional-order spots until a final convergence after a further 225 iterations.

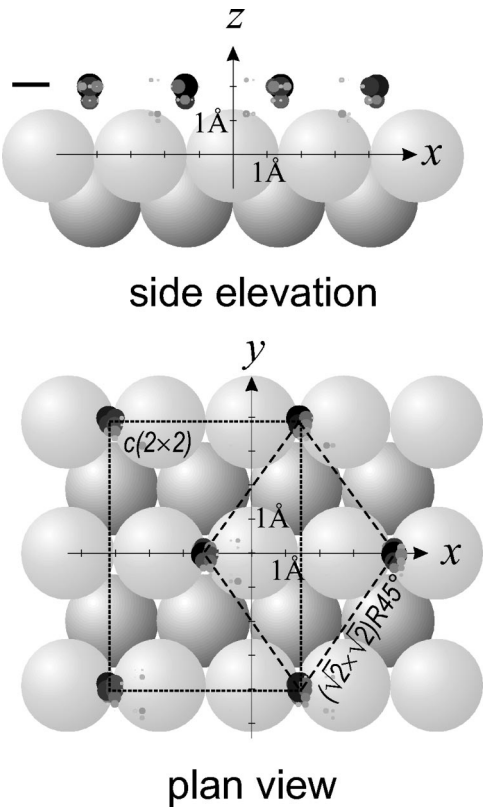


FIG. 8. Plan view and side elevation of the directly recovered $c(2\times2)$-Br/Pt(110) structure with the Br atoms adsorbed on short-bridge sites.

Two perspectives of the final distribution $\{p_j^{(575)}\}$ are shown in Fig. 8. The lower panel shows a plan view of the surface. High values of the distribution are found only at short-bridge sites in a $c(2\times2)$ lattice relative to the Pt(110) substrate. These are precisely the lattice sites suggested by the conventional LEED analysis and DFT calculations.[40] Note that these results suggest just one adatom per primitive surface unit cell. Consequently, all adatoms are also at the same height (2.0 Å) relative to the substrate, as illustrated in the side elevation (upper panel). The short black horizontal line in this panel marks the adsorbate height determined by the conventional LEED analysis. The atom distribution determined by our algorithm is found to agree well with this determination.

### B. $(3\times1)$-Br/Pt(110)

The $3\times1$ phase develops at a two-third Br coverage of the surface.[42] Again STM, DFT, and quantitative LEED have been applied to resolve the structure.[43,44] The surface unit cell is made up by two Br atoms which reside on inequivalent sites, one again in the short-bridge and the other in the long bridge site.

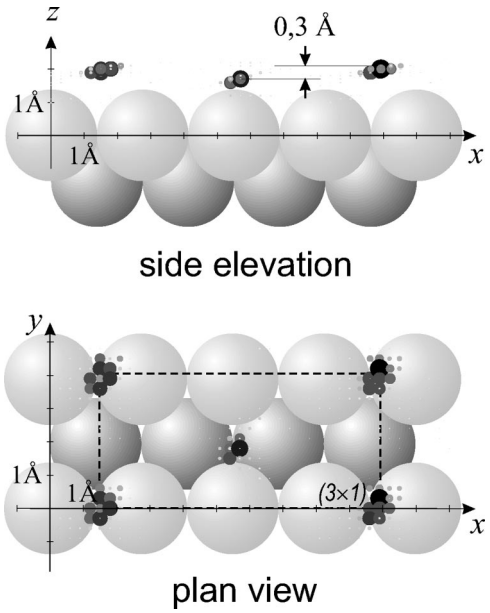


FIG. 9. Plan view and side elevation of the directly recovered $(3\times1)$-Br/Pt(110) structure with its two inequivalent Br atoms adsorbed on short- and long-bridge sites.

A similar attempt as above was made to recover this adsorbate structure by the application of our algorithm to LEED data taken at normal incidence for eight integer-order and 12 fractional-order symmetrically inequivalent beams. The algorithm was run initially to convergence after 40 iterations with just data from the integer-order spots. After the same reciprocal-space interpolation as before of the phases of the surface components of the structure factors to give starting phases of the fractional-order structure factors, and the inclusion of data from all Bragg spots (integer-order and fractional-order) the algorithm was resumed until final convergence after a further 300 iterations.

The resulting atom distribution $\{p_j^{(340)}\}$ within a surface slab with lateral extension of 0.0–12.0 Å and −0.90–4.8 Å along $x$ and $y$ axes, respectively, on a 0.30-Å grid and height 2.20 Å (resolution 0.20 Å, $d_{\min}=1.0$ Å) is shown in Fig. 9. Once again, the lower panel gives a plan view of the distribution over a little more than the $3\times1$ superstructure unit cell. Note that in this structure there are two symmetrically inequivalent atoms per $3\times1$ surface unit cell occupying two different adsorption sites (long bridge and short bridge). As Br-Pt bond lengths are almost the same for both adsorption sites,[43,44] the height of the Br atom adsorbed on the long-bridge site is lower than that for the short-bridge site by 0.3 Å (cf. side elevation in the upper panel of Fig. 9). This conclusion is supported by an independent conventional LEED analysis by which this relative difference is determined to be 0.26 Å.[43,44]

### C. (5×1)-H/Ir(001)

It has been known since the early 1980s that the clean Ir(001) surface reconstructs to form a $5\times1$ structure, whereby the top layer forms a quasihexagonal lattice, which matches the square lattice of the underlying metal layers at positions corresponding to a $5\times1$ coincidence lattice.[45–47] In the direction of the larger surface unit vector, six rows of Ir atoms of the outermost surface layer are packed into a length equal to that of five rows of the layer beneath.

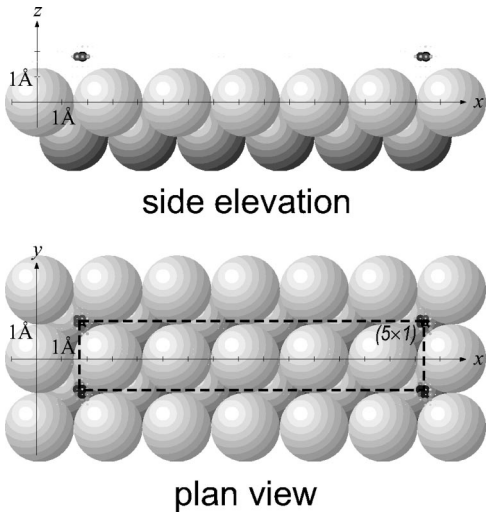


FIG. 10. Plan view and side elevation of the directly recovered $(5\times1)$-H/Ir(001).

On adsorption of H, recent conventional LEED studies showed that one of six Ir rows in the top layer becomes extracted from that layer so that its atoms reside in hollow sites of the underlying (now almost bulk terminated) Ir(001) substrate.[48,49] The extracted Ir rows are arranged in a $5\times1$ superlattice relative to the square substrate lattice. This model is corroborated by scanning tunneling microscopy studies. So we used the structure factors of an unrelaxed and unreconstructed Ir(001) surface as a reference wave $R_\epsilon$ for our maximum entropy algorithm.

Our inversion algorithm was run initially for 50 iterations with just the same LEED data in five inequivalent integer-order reflections, followed (after the usual phase-interpolation procedure for starting phases of those Bragg spots) by 50 further iterations with the inclusion also of nine inequivalent fractional-order reflections. The result is shown in Fig. 10. Obviously, the atoms of the extracted Ir rows [located 1.8 Å above the topmost Ir(001) bulk layer] occupy four-fold coordinated hollow-sites. Both the adsorption site and the adsorption height are in quantitative agreement with the conventional LEED intensity analysis.[48,49] For the recovery of the atomic distribution $\{p_l\}$ the Lagrange parameter was determined according to Eq. (17), with the constant $b$ taken to be 0.01. Due to a very low value of $\max\{p_l^{(0)}\}$ at the outset [through Eq. (19)], the initial values of the parameter $\lambda$ are rather high, but decrease rapidly down to around $\lambda=0.3$ (cf. Fig. 11). This dependency of $\lambda$ on $n$ makes the iterative procedure converge much faster than treating $\lambda$ as a constant.

## VII. DISCUSSION AND CONCLUSIONS

To date most surface crystal structures have been solved by a combination of chemical intuition, the pooling together of data from different physical probes, and by trial-and-error

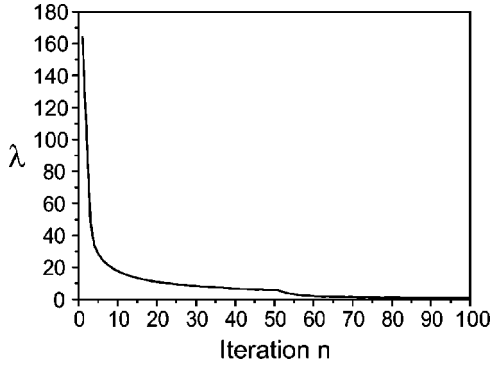


FIG. 11. Dependency of the parameter λ on the iteration step *n* for the $(5\times1)$-H/Ir(001) structure.

fitting to experimental diffraction data, of simulations of diffraction data from guessed models of the structure. The latter process invariably runs up against the exponential growth with complexity of the structure of the number of models that need to be tested. Consequently, more attention has been devoted in recent years to developing a reliable *direct* method for surface crystallography that may lead rapidly from the experimental diffraction data to the surface structure at the atomic scale. One of the ideas that has attracted attention in recent years is that of interpreting the diffraction patterns in some sense as an interference pattern between an assumed known spherical *reference wave* from an identifiable atom within a surface unit cell and the *object waves* formed by the scattering of this wave from its neighboring atoms. If such an interpretation is possible, *holographic* computer reconstruction algorithms are able to reveal the three-dimensional arrangement of the neighboring atoms relative to the reference wave source.[16] When the hologram is formed by the interference of low energy electrons, the decay of the reference wave with the inverse of distance from the source, as well as its attenuation due to inelastic scattering, generally does not allow the recovery of more than just a few atoms in the vicinity of the source.[19] Also, the existence of more than one reference wave source could lead to the superposition of more than one local atomic environment, with a consequent difficulty of interpretation.

In this paper we develop an alternative holographic interpretation for surface crystallography that promises to overcome these problems. It is based on the idea that when an external beam of radiation is directed into a surface, the radiation detected outside the sample will have scattered from not just the outermost surface layers whose structure may need to be determined, but also from parts of the underlying bulk crystal, whose structure is generally known. The calculable scattered radiation from this known part of the structure is thus identified with the reference wave and that scattered from the unknown part of the structure with the object wave. A conventional holographic algorithm would be capable of recovering the object wave from the diffraction data and a knowledge of the reference wave (which may be calculated from a knowledge of the bulk structure). We go one step farther: by writing the object wave as a linear combination of calculated components (elementary object waves) associated with a given position of an *average surface atom* on a uniform grid covering a 3D slab representing the surface unit cell, we develop an algorithm to recover the coefficients of that linear sum.

A development of this idea for surface x-ray diffraction has been described previously,[22,50,51] where the elementary object waves take the form of simple exponential functions, and the (non-negative) coefficients represent the electron density in the surface unit cell. In the present case of LEED, the components may be regarded as elements of effective (or renormalized) scattering matrices of a primitive lattice of test atoms of the 2D periodicity of the superstructure *in a given geometrical relation to the substrate*. Such effective scattering matrices may be calculated rapidly from standard LEED programs, taking account of the dominant (first-order) multiple-scattering with the substrate. Only as many such scattering matrices need be calculated as there are grid points within a symmetry-reduced sector of the surface unit cell multiplied by the number of energies at which LEED data are measured. For a given data set and a given number of real-space grid points, the computer time for the calculation is thus *independent of the structural complexity of the unit cell*. The coefficients of the expansion of these components of the object wave may be regarded as the elements of a non-negative distribution of atoms in the surface unit cell, to be determined.

In the cases of either x-ray diffraction or LEED, the relevant distribution is determined by a maximum entropy algorithm,[22] which iteratively satisfies the experimental constraints to the reciprocal-space data, while also ensuring the non-negativity of all elements of the sought distribution in real space at each iteration. The theory for x-ray diffraction was given in an earlier paper,[22] which also contains examples of the operation of the algorithm to recover the electron density of the surfaces of a number of structures from realistic simulations of surface x-ray diffraction data from a standard program.[52]

In the present paper, we extend the theory to LEED and demonstrate its application to determine the adsorption geometries of ordered adsorbates on surfaces from both simulated LEED data for $c(2\times2)$-CO/Ni(001), and experimental data from the $c(2\times2)$ and $3\times1$ phases of Br/Pt(110), and the $(5\times1)$-H/Ir(001) surface. In the case of the simulated data, the algorithm accurately recovered the very model used to calculate the LEED spectra. An application of the algorithm to experimental data recovered adsorption structures fully in agreement with the results of conventional LEED analysis.

Here we have described applications only to the recovery of the structure of adsorbates (atomic or molecular) on unreconstructed and unrelaxed (or nearly so) substrates. This enables the representation of the reference wave by the total diffracted complex amplitude from a truncated known bulk structure. Complications might be expected when the substrate itself suffers major (unknown) reconstruction or relaxation or, in other words, when the undisturbed bulk starts deeper within the sample. We expect to address such problems in future papers.

**ACKNOWLEDGEMENTS**

We gratefully acknowledge support for this work from the Deutsche Forschungsgemeinschaft (DFG) through Sonder-forschungsbereich 292, the U.S. National Science Foundation (Grant Nos. DMR-9815092, and DMR-9972958-001) and the U.S. Department of Energy (Grant Nos. DE-FG02-84ER45076 and DE-FG02-01ER45926).

[1] J. B. Pendry, *Low Energy Electron Diffraction* (Academic, London, 1974).
[2] M. A. Van Hove, W. H. Weinberg, and C.-M. Chan, *Low Energy Electron Diffraction* (Springer-Verlag, Berlin, 1986).
[3] K. Heinz, Rep. Prog. Phys. **58**, 637 (1996).
[4] M. A. Van Hove and S. Y. Tong, *Surface Crystallography by LEED* (Springer, Berlin, 1979).
[5] J. B. Pendry, K. Heinz, and W. Oed, Phys. Rev. Lett. **61**, 2953 (1988).
[6] P. G. Cowell and V. E. Carvalho, Surf. Sci. **187**, 175 (1987).
[7] P. J. Rous, Surf. Sci. **296**, 358 (1993).
[8] M. Kottcke and K. Heinz, Surf. Sci. **376**, 352 (1997).
[9] R. Döll and M. A. Van Hove, Surf. Sci. **355**, L393 (1996).
[10] P. J. Rous, J. B. Pendry, D. K. Saldin, K. Heinz, K. Müller, and N. Bickel, Phys. Rev. Lett. **57**, 2951 (1986).
[11] M. A. Van Hove, W. Moritz, H. Over, P. J. Rous, A. Wander, A. Barbieri, N. Materer, U. Starke, and G. A. Somorjai, Surf. Sci. Rep. **19**, 191 (1993).
[12] V. Blum and K. Heinz, Comput. Phys. Commun. **134**, 392 (2001).
[13] D. Gabor, Nature (London) **161**, 777 (1948).
[14] A. Szöke, in *Short Wavelength Coherent Radiation: Generation and Applications*, edited by D. J. Attwood and J. Boker, AIP Conf. Proc. No 147 (AIP, New York, 1986).
[15] D. K. Saldin and P. L. de Andres, Phys. Rev. Lett. **64**, 1270 (1990).
[16] K. Heinz, A. Seubert, and D. K. Saldin, J. Phys.: Condens. Matter **13**, 10647 (2001).
[17] D. K. Saldin, K. Reuter, P. L. De Andres, H. Wedler, X. Chen, J. B. Pendry, and K. Heinz, Phys. Rev. B **54**, 8172 (1996).
[18] C. M. Wei, S. Y. Tong, H. Wedler, M. A. Mendez, and K. Heinz, Phys. Rev. Lett. **72**, 2434 (1994).
[19] K. Reuter, J. Bernhardt, H. Wedler, J. Schardt, U. Starke, and K. Heinz, Phys. Rev. Lett. **79**, 4818 (1997).
[20] Various holographic methods have been reviewed in a recent special volume: J. Phys.: Condens. Matter **13**, 47 (2001)
[21] V. L. Shneerson, D. L. Wild, and D. K. Saldin, Acta Crystallogr. Sect. A: Found. Crystallogr. **57**, 163 (2001).
[22] D. K. Saldin, R. J. Harder, H. Vogler, W. Moritz, and I. K. Robinson, Comput. Phys. Commun. **137**, 12 (2001).
[23] D. K. Saldin, A. Seubert, and K. Heinz, Phys. Rev. Lett. **88**, 115507 (2002).
[24] C. Giacovvazzo, *Direct Methods in Crystallography* (Academic, London, 1980).
[25] A. Szöke, Phys. Rev. B **47**, 14044 (1993).
[26] D. S. Sivia, *Data Analysis: A Bayesian Tutorial* (Oxford University Press, Oxford, 1996).
[27] E. T. Jaynes, Phys. Rev. **106**, 620 (1957).
[28] S. F. Gull and G. J. Daniell, Nature (London) **272**, 686 (1978).
[29] D. M. Collins, Nature (London) **298**, 49 (1982).
[30] D. M. Collins and M. C. Mahar, Acta Crystallogr. Sect. A: Found. Crystallogr. **39**, 252 (1983).
[31] G. Bricogne, Acta Crystallogr. Sect. A: Found. Crystallogr. **40**, 410 (1984).
[32] G. Bricogne, Acta Crystallogr. Sect. A: Found. Crystallogr. **44**, 517 (1988).
[33] G. Bricogne, in *Maximum Entropy in Action*, edited by B Buck and V A Macaulay (Oxford University Press, Oxford, 1991), p. 187.
[34] C. J. Gilmore, Acta Crystallogr. Sect. A: Found. Crystallogr. **52**, 561 (1996).
[35] G. Bricogne, Acta Crystallogr., Sect. D: Biol. Crystallogr. **49**, 37 (1993).
[36] L. D. Landau and E. M. Lifshitz, *Statistical Physics* (Pergamon, New York, 1980).
[37] This *quasi-dynamical* approximation has also been employed successfully in conventional LEED analyses, see e.g. N. Bickel and K. Heinz, Surf. Sci. **163**, 435 (1985).
[38] This is necessary to ensure that the incident electrons are absorbed the same amount in propagating to the substrate.
[39] M. Sowwan, Y. Yacoby, J. Pitney, R. MacHarrie, M. Hong, J. Cross, D. A. Walko, R. Clarke, R. Pindak, and E. A. Stern, Phys. Rev. B **66**, 205311 (2002).
[40] V. Blum, L. Hammer, K. Heinz, C. Franchini, J. Redinger, K. Swamy, C. Deisl, and E. Bertel, Phys. Rev. B **65**, 165408 (2002).
[41] K. Swamy, P. Hanesch, P. Sandl, and E. Bertel, Surf. Sci. **466**, 11 (2000).
[42] C. Deisl, K. Swamy, R. Beer, A. Menzel, and E. Bertel, J. Phys.: Condens. Matter **14**, 4199 (2002).
[43] C. Deisl, S. Walter, C. Franchini, K. Swamy, E. Bertel, L. Hammer, K. Heinz, and J. Redinger, Verhandl. DPG (VI) **37/1**, O22.5 (2002).
[44] C. Deisl, K. Swamy, E. Bertel, C. Franchini, J. Redinger, S. Walter, L. Hammer, and K. Heinz, (unpublished).
[45] M. A. Van Hove, R. J. Koestner, P. C. Stair, J. P. Biberian, L. L. Kesmodel, I. Bartos, and G. A. Somorjai, Surf. Sci. **103**, 218 (1981).
[46] E. Lang, K. Müller, K. Heinz, M. A. Van Hove, R. J. Koestner, and G. A. Somorjai, Surf. Sci. **127**, 347 (1982).
[47] N. Bickel and K. Heinz, Surf. Sci. **163**, 435 (1985).
[48] L. Hammer, W. Meier, A. Schmidt, and K. Heinz, *Proceedings of the Symposium on Surface Science 2002, St. Christoph am Arlberg, Austria, March 3-9, 2002*.
[49] A. Schmidt, W. Meier, L. Hammer, and K. Heinz, Verhandl. DPG (VI) **37/1**, O32 (2002).
[50] D. K. Saldin, R. J. Harder, V. L. Shneerson, and W. Moritz, J. Phys.: Condens. Matter **13**, 10689 (2001).
[51] D. K. Saldin, R. J. Harder, V. L. Shneerson, and W. Moritz, J. Phys.: Condens. Matter **14**, 4087 (2002).
[52] E. Vlieg, J. Am. Ceram. Soc. **33**, 401 (2000).